RESEARCH ARTICLE | MAY 02 2023

Reducing the impact of adaptive optics lag on optical and quantum communications rates from rapidly moving sources

Kai Sum Chan ; H. F. Chau

AIP Advances 13, 055201 (2023)
https://doi.org/10.1063/5.0149695

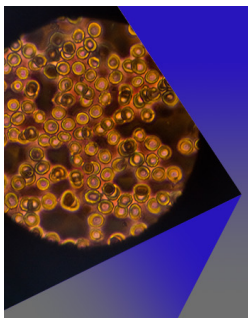

Reducing the impact of adaptive optics lag on optical and quantum communications rates from rapidly moving sources

Cite as: AIP Advances 13, 055201 (2023); doi: 10.1063/5.0149695
Submitted: 7 March 2023 • Accepted: 7 April 2023 •
Published Online: 2 May 2023

Kai Sum Chan[a] and H. F. Chau[b]

AFFILIATIONS

Department of Physics, University of Hong Kong, Pokfulam Road, Hong Kong, China

[a]**Present address:** Quantum Bridge Technologies Inc., 100 College Street, Toronto, Ontario M5G 1L5, Canada and National Research Council of Canada, Ottawa, Ontario K1A 0R6, Canada.
[b]**Author to whom correspondence should be addressed:** hfchau@hku.hk

ABSTRACT

Wavefront of light passing through the turbulent atmosphere gets distorted. This causes signal loss in free-space optical communication as the light beam spreads and wanders at the receiving end. Frequency and/or time division multiplexing adaptive optics (AO) techniques have been used to conjugate this kind of wavefront distortion. However, if the signal beam moves relative to the atmosphere, the AO system performance degrades due to high temporal anisoplanatism. Here, we solve this problem by adding a pioneering beacon that is spatially separated from the signal beam with time delay between spatially separated pulses. More importantly, our protocol works irrespective of the signal beam intensity and, hence, is also applicable to secret quantum communication. In particular, using semi-empirical atmospheric turbulence calculation, we show that for low earth orbit satellite-to-ground decoy state quantum key distribution with the satellite at zenith angle $<30^{\circ}$, our method increases the key rate by at least 215% and 40% for satellite altitudes of 400 and 800 km, respectively. Finally, we propose a modification of the existing wavelength division multiplexing systems as an effective alternative solution to this problem.

I. INTRODUCTION

Optical free-space communications and astronomical imaging are affected by atmospheric turbulence due to fluctuation of air density, pressure, and temperature. This turbulence induces a time-dependent inhomogeneous refractive index in air, distorting the wavefront of electromagnetic waves. Hence, the light beam spreads and wanders at the detection end causing signal loss. The high-fidelity signal or image is obtained if one could adaptively and dynamically conjugate the optical path difference caused by the wavefront distortion. Adaptive optics (AO) is a well-established method to achieve this goal.[1–3] In the most basic AO setup, a deformable mirror (DM) is used to collect the light signal, and a beam splitter is placed in front of the signal detector acting as a signal sampler to divert some signal light to a wavefront sensor. The detection result of this sensor is then used to estimate the wavefront distortion. Finally, one can adaptively conjugate this estimated distortion via fast feedback control of the DM through actuators to obtain a high-fidelity signal or image.[1–4]

Many variants of this basic setup have been proposed and used in the field. For instance, one may replace the beam splitter by a wavelength selector plus an additional beacon beam emitting light with a different wavelength from that of the signal beam. This wavelength-division multiplexing (WDM) setup is effective if the wavelengths of the two beams are close enough so that the wavefront distortion inferred from the beacon beam is close to that of the signal beam. At the same time, the wavelength difference is big enough to avoid crosstalk between the two beams. Another variant is to use the time-division multiplexing (TDM) method in which the beam splitter is replaced by an optical switch and a pulsed beacon beam.[3] We remark that in most WDM and TDM setups, the beacon and the signal beams spatially coincide. In order to work, the WDM and TDM methods must use a sufficiently high-intensity beacon beam so that the wavefront sensor can detect enough

photons per unit time to estimate the wavefront distortion accurately. In contrast, the brightness of the signal source is irrelevant as far as AO correction is concerned. That is to say, both WDM and TDM methods work for low intensity signal sources, including most quantum signal sources used in secure quantum communication. In fact, WDM has been used in a few recent quantum communication experiments.[5,6]

A new challenge is faced if the signal source moves sufficiently fast relative to the atmosphere. This increases the temporal angular distance between the optical path of the beacon and the corresponding path of the signal due to AO lag. The temporal anisoplanatism induced by the movement of the source greatly degrades the system's performance. Our method to tackle this challenge is inspired by astronomical imaging of dim celestial objects. Recall that astronomers use an artificial high intensity laser guide star placed angularly close to the dim astronomical object as the beacon source to replace the role of the diverted signal light.[1,2,7] With this inspiration, we solve the moving source problem by using two sets of spatially separated artificial sources emitting at the same or nearly the same wavelength—a set of (pulsed) pioneer beacon source(s) to perform effective AO correction and another set of time-delayed (pulsed) signal source(s) for the actual optical communication. In essence, our proposal is a time-delayed spatial multiplexing protocol. This protocol can also be interpreted as a time-based AO pre-compensation scheme in the sense that the DM pre-deforms before the signal arrives. This is different from another type of AO pre-compensation scheme in uplink satellite communication in which the signal is pre-shaped before sending to the satellite.[8,9]

For concrete illustration, we consider the following prototype from now on although the general concept works in a much wider context. As shown in Fig. 1, we consider the satellite-to-ground communication setup with both the beacon and signal sources fixed on a low earth orbit (LEO) satellite together with a stationary ground-based receiver telescope. By the pioneer beacon source, we mean that the beacon beam is put in front of the signal beam along the direction of motion of the satellite relative to the ground. Furthermore, we fire each pulsed pioneer beacon beam shortly before firing the corresponding pulsed signal beam. In doing so, the beacon beam acts like a pioneer that probes the wavefront distortion of an optical path that will shortly be traveled by the signal beam. Specifically, if the two beams move sufficiently rapidly relative to the detector(s), the pulsed pioneer beacon beam and the corresponding delayed pulsed signal beam can be made to travel along essentially the same optical path by carefully tuning the delay time. Consequently, our time-based AO pre-compensation technique should achieve almost the same level of AO correction for stationary sources without spatial multiplexing. As the two light sources are multiplexed spatially, their signals can be separated effectively by focusing the light beams, provided that the angular separation of their images after applying AO correction is greater than the resolving power of the ground-based telescope and that the crosstalk between them is sufficiently small. In fact, a recent experiment using the 1 m telescope in Mount Stromlo Observatory plus AO imaging technique succeeded to image an artificial satellite down to 85 cm in size at 1000 km range.[10] This implies that using the telescope with an aperture larger than about 1 m, our prototype is able to resolve and separate the pioneer beacon and signal beams mounted on a typical-sized artificial satellite.

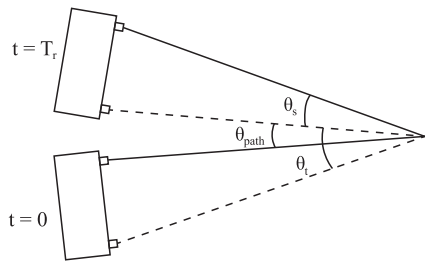

FIG. 1. Satellite location and beams' path at $t = 0$ and $t = T_r$. Here, θ_s is the angular separation of the pioneer beacon and signal beams (as observed from the receiver), and θ_t is the angle traveled by the signal (pioneer beacon) beam's path from $t = 0$ to $t = T_r$ [see the solid (dash) lines]. In addition, θ_{path} is the angle between the pioneer beacon beam's path (solid line at $t = 0$) and the delayed signal beam's path (dash line at $t = T_r$).

Note that we study this prototype because this is one of the most challenging situations in realistic applications. As the effectiveness of our approach does not depend on the nature of the signal light source, so by the same logic, we choose our signal source to be a phase-randomized weak coherent quantum source performing decoy state quantum key distribution (QKD). In this way, we could demonstrate the strength of our approach and compare it with the existing ones. In fact, the free-space channel is used in quantum communication because it has a lower attenuation rate than optical fibers of the same length.[11] No wonder why several pioneering demonstrations of long distance free-space QKD, including ground-to-ground and satellite-to-ground ones, have been reported.[5,6,12,13] For free-space QKD, existing AO technologies are able to increase the key rate by reducing the widening effect and spatial noise of the signal so that the system can get a higher yield or coupling efficiency even in daytime.[6,14] To the best of our knowledge, all AO-based free-space QKD experiments to date use WDM.[5,6] A drawback of this approach is that the different wavefront distortions experienced by the beacon and signal beams generally increase with communication distance. This could lower the yield and key rate when this distance is long. More importantly, both WDM and TDM suffer from huge temporal anisoplanatism.

We begin by presenting the atmospheric model and system parameters used in our investigation in Sec. II. Then, in Sec. III, we introduce our time-delayed spatial multiplexing method of time-based AO pre-compensation that uses a pulsed pioneer beacon beam plus a time-delayed pulse signal beam. We also analyze its effectiveness in transmitting information through the dynamical atmosphere. In Sec. IV, we show the schematic design of the spatial multiplexing system and discuss the crosstalk due to the pioneer beacon. With the above preparatory works, we study the performance of our scheme for the case when crosstalk between the pioneer beacon and the signal beams can be ignored in Sec. V. Specifically, for the case of our concrete illustrative example, our scheme always gives a higher Strehl ratio and transmission efficiency over those that use pure TDM or WDM. In addition, we analyze the situation in which crosstalk cannot be ignored in Sec. VI. There we compute the secret

key rate of decoy state BB84 QKD that is optimized over signal beam parameters. Again, we find that for our concrete illustration, our scheme always gives a higher provably secure key rate over pure TDM and WDM protocols. By semi-empirical calculation, we find that for the satellite at zenith angle <30°, the provably secure QKD key rate of our scheme is increased by at least 215% and 40% when the satellite altitude is 400 and 800 km, respectively. We also find that generally a greater key rate improvement is obtained when the system bandwidth is lower, the distance between the pioneer beacon and signal beams is higher, and the angular speed of the satellite relative to the ground detector is faster. As our setup is new and its construction is engineering demanding, a compromise is to upgrade existing WDM systems to combine the beacon and signal beams. We report the performance of this modification in Sec. VII. We find that for the zenith angle less than about 45°, the provably secure key rate of this modification is at least 90% of our spatial multiplexing prototype reported in Sec. VI, making it an attractive practical alternative. Finally, we summarize our findings in Sec. VIII. The present work is based on our recent patent application[15] and the Master thesis of one of the authors.[16]

II. ATMOSPHERIC MODEL AND SYSTEM PARAMETERS OF THE FREE-SPACE COMMUNICATION CHANNEL

A. Atmospheric model

The Fried parameter r_0 is one of the most important quantity characterizing the atmospheric coherence diameter due to turbulence.[17] In unit of meters, its value varies with the altitude and the zenith angle according to the equation

$$r_0 = \left[0.423k^2 \sec(\zeta) \int_0^{h_{\text{alt}}} C_n^2(h)\, dh\right]^{-3/5}, \tag{1}$$

where ζ is zenith angle, k is the wavenumber of the light measured in m^{-1}, h_{alt} is the altitude of the source measured in meters, and $C_n^2(h)$ is the refractive index structure parameter at altitude h. Here, we assume that $C_n^2(h)$ follows the Hufnagel–Valley model,[18] namely,

$$C_n^2(h) = 0.005\,94\left(\frac{w}{27}\right)^2\left(\frac{h}{10^5}\right)^{10}\exp\left(-\frac{h}{1000}\right) + 2.7\times10^{-16}\exp\left(\frac{-h}{1500}\right) + 1.7\times10^{-14}\exp\left(\frac{-h}{100}\right), \tag{2}$$

with h measured in meters. In most literature, $w = 21$ m/s is the pseudo-wind speed, taken to be the average wind speed of the jet stream.[18] We stress that Eqs. (1) and (2) are valid for a source that is either stationary or moving relative to the detector.

Isoplanatic angle θ_0 and Greenwood frequency f_G are two quantities that can be used to characterize the spatial and temporal limits in AO. At the receiving end, light rays coming from a cone with an angle much smaller than θ_0 has about the same optical path length. f_G, which is the reciprocal of the beam wandering time, is an effective way to approximately quantify the rate of change of turbulence.[3,19] Clearly, for a stationary source, AO is effective only if the angular separation between the (pulsed) beacon beam and the (pulsed) signal beam is much less than θ_0. Moreover, the time delay between these two pulsed beams is much less than $1/f_G$. These two quantities can be computed via $C_n^2(h)$ through

$$\theta_0 = \left[2.913k^2 \sec^{8/3}(\zeta) \int_0^{h_{\text{alt}}} h^{5/3} C_n^2(h)\, dh\right]^{-3/5} \tag{3}$$

and

$$f_G = \left[0.1022k^2 \sec(\zeta) \int_0^{h_{\text{alt}}} v^{5/3}(h) C_n^2(h)\, dh\right]^{3/5}, \tag{4}$$

where $v(h)$ is the wind speed at altitude h.[3,19]

For the case of moving source, $v(h)$ in Eq. (4) is given by

$$v(h) = v_{\text{wind}}(h) + v_{\text{app}}(h), \tag{5}$$

where $v_{\text{wind}}(h)$ is the natural wind speed and $v_{\text{app}}(h)$ is the apparent wind speed due to the movement of the source. This assumption of simply adding two scalar speeds in Eq. (5) is justified when the moving source is mounted on a LEO satellite because it moves at great angular speed so that $v_{\text{app}} \gg v_{\text{wind}}$. We further assume that the natural wind speed follows the altitude-dependent Bufton wind profile,[20]

$$v_{\text{wind}}(h) = v_g + 30\exp\left[-\left(\frac{h-9400}{4800}\right)^2\right]. \tag{6}$$

Here, v_g is the natural wind speed and is taken to be 5 m/s in our analysis.[20]

B. LEO satellite and receiving end telescope

LEO satellite-to-ground communication is considered in this paper because of its low aperture-to-aperture loss and high speed features. For simplicity, we assume that the satellite is moving in a circular orbit passing through the zenith of the detector. Furthermore, we simply calculations by ignoring the rotation of the Earth as the orbital period of a LEO satellite is much shorter than 1 day. Then, the distance between the transmitter and the receiver can be expressed as

$$z(\zeta) = \sqrt{h_{\text{alt}}^2 + 2h_{\text{alt}}R_\oplus + R_\oplus^2\cos^2(\zeta)} - R_\oplus\cos(\zeta), \tag{7}$$

where $R_\oplus$ is the Earth radius. In addition, the angular slewing rate is equal to

$$\omega_s = \left[\frac{GM_\oplus}{h_{\text{alt}}^2(h_{\text{alt}}+R_\oplus)}\right]^{1/2}\cos^2(\zeta), \tag{8}$$

where G is the universal gravitational constant and $M_\oplus$ is the Earth mass. Clearly, the apparent wind speed v_{app} at height h equals

$$v_{\text{app}}(h) = \omega_s h. \tag{9}$$

To illustrate this idea, we consider the satellite moving at two different altitudes, namely, $h_{\text{alt}} = 400$ and 800 km, in this paper.

At the receiving end, the aperture coupling efficiency can be approximated by using Gaussian beam equation[21]

$$\eta_{\text{geo}}(\omega) = 1 - \exp\left[-\frac{1}{2}\frac{D^2}{\omega^2(\lambda, z(\zeta))}\right], \tag{10}$$

where D is the diameter of the telescope aperture, λ is the wavelength, z is the propagation distance, and the waist function ω equals

$$\omega^2(\lambda, z(\zeta)) = \omega_0^2\left[1 + \frac{z(\zeta)^2}{z_R^2(\lambda)}\right], \tag{11}$$

with $z_R = \pi\omega_0^2/\lambda$ being the Rayleigh range and $\omega_0 \equiv 0.7D_T/2$ being the beam waist. We take $D_T = 0.05$ m as the diameter of the transmitter aperture. The telescope parameters used are based on a real telescope in the Lulin observatory.[22] It is a Cassegrain telescope with diameter $D = 1.03$ m, secondary mirror diameter 0.36 m, and effective focal length $f = 8$ m.

C. Wavelength selection

A shorter wavelength gives better quantum channel performance due to the spatial filtering strategies, geometric coupling, and size of the focus spot.[21] This conclusion is consistent with the implicit dependence of η_{geo} on λ, as shown in Eqs. (10) and (11). Moreover, we assume that there is a field stop (FS) in front of the signal receiver to filter the background noise. The size of this FS is taken as the diffraction limit of the signal beam. In this configuration, the FS can filter most of the background light, while 84% of the signal can pass through (if the signal is not distorted). Since the spot size of the beam is proportional to its wavelength, a longer wavelength increases the size of the FS and the number of background photons that pass through.

Based on these factors and some site-specific conditions, Gruneisen *et al.* used 780 nm as the wavelength of the signal beam and 808 nm as the wavelength of the beacon in their daytime quantum communication experiment.[6] As our paper focuses more on quantum scenarios, we follow them by fixing the wavelengths of both the signal and beacon beams in our time-delayed spatial multiplexing prototype to 780 nm. For the WDM systems that we use for performance comparison, the beacon wavelength used is set to 808 nm.

III. REDUCING THE ANISOPLANATISM BY USING A PIONEER BEACON

Anisoplanatism occurs when there is an angular difference θ_{path} between the beacon and the signal. It increases the wavefront variance σ^2_{path} and hence degrades the performance of the AO system. This variance can be expressed as[3]

$$\sigma^2_{\text{path}} = \left(\frac{\theta_{\text{path}}}{\theta_0}\right)^{5/3}, \tag{12}$$

where θ_{path} is the angle between the beacon beam path and its corresponding signal beam path and θ_0 is the isoplanatic angle calculated using Eq. (3). There are two origins for anisoplanatism. Spatial anisoplanatism is induced by the spatial angular separation,

$$\theta_s = \frac{L}{z(\zeta)}, \tag{13}$$

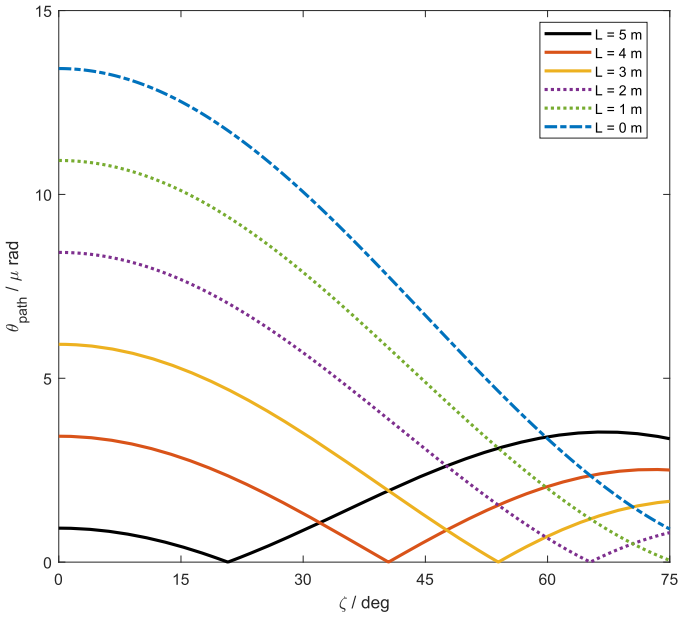

(a) $h_{\text{alt}} = 400$ km

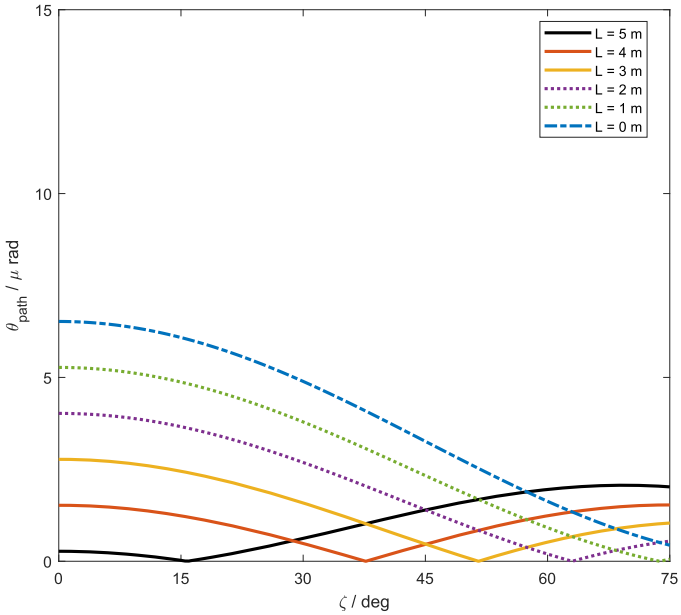

(b) $h_{\text{alt}} = 800$ km

FIG. 2. Total angular difference θ_{path} between the optical paths defined by Eq. (16). The black solid, red solid, yellow solid, purple dotted, green dotted, and blue dashed-dotted curves are computed with spatial separation L being 5, 4, 3, 2, 1, and 0 m, respectively. Note that the case without spatial multiplexing is the one with $L = 0$ m.

of the beams. On the other hand, temporal angular separation refers to the angle between the optical paths at two different timestamps, and the time duration is the response time (in other words, the AO lag time) T_r of the system. The temporal angle can be expressed as

$$\theta_t = \omega_s T_r. \tag{14}$$

We fix the delay time T_r as the time taken between 10% and 90% of steady-state output. As we model the system as an RC filter, T_r can be expressed as

$$T_r = \frac{0.35}{f_c}, \tag{15}$$

where $f_c = 500$ Hz is the 3 dB bandwidth of the whole AO feedback loop system. We further checked that this delay time T_r is much shorter than $1/f_G$. Although our design increases the spatial angle θ_s, the total anisoplanatism actually decreased as the beacon is located in front of the signal beam. This is because the angle that contributes to anisoplanatism is

$$\theta_{\text{path}} = |\theta_t - \theta_s| \tag{16}$$

(see Fig. 1 for an illustration.)

If the beacon and signal beams are not spatially separated, $L = 0$ m and, hence, $\theta_s = 0$ rad. As shown in Figs. 2 and 3, spatially separating the two beams generally decreases both θ_{path} and σ^2_{path} for zenith angle $\zeta \lesssim 60^\circ$ and $L \leq 5$ m. This demonstrates the reduction of anisoplanatism by using a pioneer beacon beam. Moreover, from Eqs. (7), (8), (13), and (14), it is easy to check that $d(\theta_t - \theta_s)/d\zeta < 0$ for any reasonable parameters for a LEO satellite. No wonder why Fig. 2 shows that θ_{path} decreases as ζ increases until reaches 0 rad. Beyond this point, θ_{path} goes up again. That is to say, for any fixed h_{alt}, L, and T_r, there is a specific zenith angle ζ whose corresponding θ_{path} and, hence, anisoplanatism vanish. (In reality, $\theta_{\text{path}} \approx 0$ rad for this set of parameters due to all the approximations made in the calculation.) In principle, we can artificially lengthen the delay time T_r or shorten the spatial separation L between the beacon and signal beams to fix θ_{path} to its optimal value. However, this changes the bandwidth and crosstalk calculation. For simplicity, this kind of adjustment is not discussed in this paper. Instead, we are going to report the effects of this type of adjustment in our follow up work. Note that even for the region that θ_{path} is increasing with ζ, our design is still better than systems that are without spatial separation.

To summarize, our signal pulse trick can reduce anisoplanatism, as shown in Fig. 3. We expect this spatial separation method to be effective in obtaining a high-fidelity signal through AO. In Sec. V, σ^2_{path} is used to show that this is indeed the case.

IV. THE ADVANTAGE OF SPATIAL MULTIPLEXING IN OUR SETUP

From the discussion of Sec. III, we expect that the path angle reduction feature in our setup is compatible with WDM and TDM systems in the sense that the pioneer beam setup can be built on top of them to reduce the anisoplanatism. However, we can further improve the AO system by using spatial multiplexing. As the beacon beam is physically separated from the signal beam, they can be distinguishable spatially. The setup itself is a spatial multiplexing system, which has two advantages compared to pure WDM and TDM systems. First, the wavelength of the sources can be the same so that chromatic effects can be ignored. Second, there is no need to temporally interlace the signal pulses with beacon pulses. For our LEO satellite setup parameters, the two beams can be spatially resolved using the AO technology because the same technology can image a satellite at the 1000 km range through a 1 m telescope.[10]

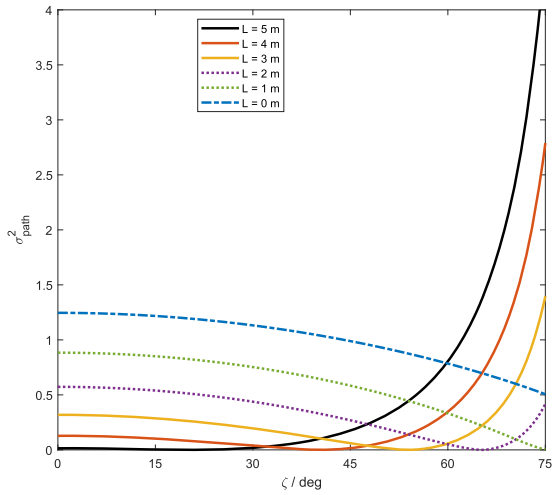

(a) $h_{\text{alt}} = 400$ km

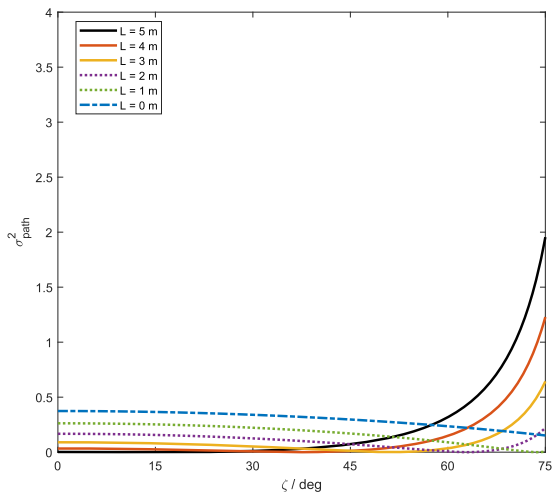

(b) $h_{\text{alt}} = 800$ km

FIG. 3. The wavefront variance σ^2_{path} due to anisoplanatism. The curves are labeled in the same way as in Fig. 2. Note that the case without spatial multiplexing is the one with $L = 0$ m.

A. Design of the beacon and signal beams

Recall that the intuition of our improved method is that two physically nearby light beams of similar frequency pass through more or less the same air column at more or less the same time and should be distorted in roughly the same way. Hence, a wavefront correction method based solely on the signal received by a wavefront sensing module that detects the pioneer beacon source beam should be able to correct both light beams at the same time with high fidelity.

Figure 4 shows the schematic of the spatial multiplexing AO system. It consists of two physically nearby sources as well as a wavefront sensing module that detects the beacon source beam plus a nearby signal detection module that detects the signal source beam(s). To reduce photon loss in long distance communication, each of the beam source is placed at the focus of the telescope on the satellite so that the emitted light beam close to the source can be well approximated by the traveling plane wave. Our hope is that with this spatial configuration, the optical paths of the two set of sources with the same or almost the same wavelength should experience more or less the same wavefront distortion. The wavefront correction then goes as follows: The beacon detection module estimates the atmospheric distortion and generates feedback signals to the control system. Then, the control system drives the actuators of the DM in the AO system. This should correct the wavefront distortion of the beacon beam as well as the possibly much weaker signal source beam simultaneously, provided that the delay time T_r between the two beams is much shorter than $1/f_G$. Surely, in order to work, the two set of sources must be placed sufficiently far apart so that the crosstalk between the beacon and signal source(s) due to effects such as diffraction and scattering is negligible.

The spatial configuration of our method is similar to the standard artificial guide star technique used in observational astronomy.[23] Note, however, that there are two major differences. First, all sources we used are artificial. Second, our beacon source is placed physically closed (and not just close in terms of apparent angular separation) to the signal source(s). We remark that this spatial configuration works not just for secure quantum communications. It is directly applicable to classical optical communication in free-space as well. In this case, the intensity of the signal source(s) need not be low. In addition, our method is applicable to ground-based, air-to-ground as well as satellite-to-ground communications, stationary as well as moving sources relative to the sensing and detecting modules. Furthermore, a nice feature of our method is that the signal transmission rate will then be independent of the beacon source.

B. Minimum physical distance between the beacon and signal sources

The minimum possible distance between the beacon and signal sources is determined by both the resolving power of the optics and the level of crosstalk between the two sets of sources. Note that upon successful AO correction, the center of the image of the beacon beam should be around the center of the optically sensitive surface of the wavefront sensing module. We put a field stop in the signal detection module to filter the noise spatially. Naturally, we set the radius of the field stop to the diffraction limit of the signal detection module.[14] The diffraction pattern depends on the structure of the telescope. In our concrete illustration, we use a 1.03 m Cassegrain telescope whose parameters are taken from a real telescope in the Lulin Observatory.[22] The light intensity of the beacon beam at a distance x away from the center equals

$$I_{\mathrm{R}}(x) \approx I_{\mathrm{R}}(0)\left(\frac{f\lambda}{\pi Dx}\right)^2\left[J_1\left(\frac{\pi Dx}{f\lambda}\right) - bJ_1\left(\frac{b\pi Dx}{f\lambda}\right)\right]^2, \tag{17}$$

where f is the effective local length of the telescope, $b = 0.36/1.03$ is ratio of the diameters of the secondary to primary mirrors of the Cassegrain telescope used, $I_{\mathrm{R}}(0) \approx 2\epsilon_0 c\mathcal{E}_{\mathrm{R}}^2\pi^2(D/2)^4/R^2$, and $J_1(\cdot)$ is the order one Bessel function of the first kind. Hence, the total light energy flux of the beacon beam imparted on the optically sensitive surface of the signal detection module is $\iint_{\mathrm{FS}} I_{\mathrm{R}}(x)dA$ where the integral is over the area of the field stop of the signal detection module. For example, when $L = 2$ m, $\iint_{\mathrm{FS}} I_{\mathrm{R}}(x)dA = 4.36 \times 10^{-15} I_{\mathrm{R}}(0)$. The

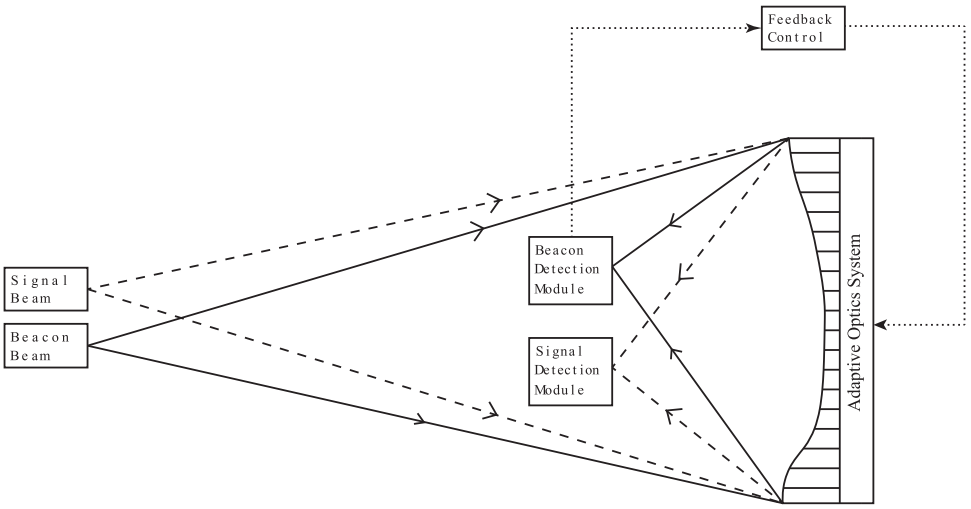

FIG. 4. Schematic diagram of the AO communication system with spatially separated beacon and signal beams.

minimum distance should be set according to the required decay from the beam center. Otherwise, stray beacon beam photons will seriously affect the signal detection statistics.

C. Scattering noise by the strong beacon beam

The scattering caused by the strong beacon beam will affect the background noise of the system and, hence, in satellite-to-ground QKD application, the final secret key rate. Some photons from the beacon may enter the signal receiving module and create errors. Here, we estimate the scattering by the strong laser in the clear sky scenario. We use sky-scattering noise to get a rough estimate on the laser scattering noise. The equation for calculating the number of sky-noise photons entering the system is given by[14]

$$N_b = \frac{H_b(\lambda)\Omega_{\mathrm{FOV}}\pi D_R^2\lambda\Delta\lambda\Delta t}{4hc}, \tag{18}$$

where H_b in W m^{-2} sr μm is the sky radiance, $\Omega_{\mathrm{FOV}} = \pi\Delta\theta^2/4$ is the solid-angle field of view with a field stop, D_R is diameter of the receiver primary optic, $\Delta\lambda$ equals to the spectral filter bandpass in μm, and Δt is the photon integration time of the receiver measured in meters. Furthermore, $\Delta\theta$ is calculated by D_{FS}/f, with D_{FS} being the diameter of the field stop. We assume $\Delta\lambda = 1$ μm as both beams use the same or nearly the same wavelength, and the spectral filter is not able to block the photons from the beacon beam.

In astrophotography, a bright star that is close to target can be used as a beacon to probe the channel. Therefore, the brightness of the beacon laser should be similar to a bright star. The sky radiance caused by the laser can be estimated by the sky radiance by the stars. Typical sky radiance is about 1.5×10^{-5} W m^{-2} sr μm under moonless clear night condition.[24] Using the parameters mentioned above and letting $\Delta t = 1$ ns, the probability of receiving a beacon photon will be in the order of 10^{-8}, which is good enough, in practice.

V. COMPARISON OF PERFORMANCE OF OUR PROTOTYPE WITH THOSE USING PURE TDM AND WDM

A. The Strehl ratio

The Strehl ratio S is a well-known metric to determine the turbulence strength and performance of optical systems. It is defined as the ratio of the peak intensity of a distorted beam spot and the peak intensity of the beam with no distortion. If the Strehl ratio equals to one, the wavefront is not aberrated. Without using AO, the Strehl ratio of the signal is[3]

$$S_{\mathrm{aber}} = \left[1 + \left(\frac{D}{r_0}\right)^{5/3}\right]^{-6/5}. \tag{19}$$

When AO is used, the performance of the system can be estimated by[3]

$$S_{\mathrm{i}} = \exp\left(-\sigma_{\mathrm{i}}^2\right), \tag{20}$$

where S_{i} is the Strehl ratio of system i and σ_i^2 is the corresponding wavefront variance, which leads to system performance degradation. Here, we compare three systems, namely, those using time-delayed spatial multiplexing, pure TDM, and pure WDM. Their wavefront variance can be written as[3,25]

$$\sigma_{\mathrm{SS}}^2 = \sigma_{\mathrm{band}}^2 + \sigma_{\mathrm{path,SS}}^2, \tag{21}$$

$$\sigma_{\mathrm{TDM}}^2 = \sigma_{\mathrm{band}}^2 + \sigma_{\mathrm{path},\overline{\mathrm{SS}}}^2, \tag{22}$$

and

$$\sigma_{\mathrm{WDM}}^2 = \sigma_{\mathrm{band}}^2 + \sigma_{\mathrm{path},\overline{\mathrm{SS}}}^2 + \sigma_{\mathrm{d}}^2 + \sigma_{\mathrm{ch}}^2 + \sigma_{\phi}^2, \tag{23}$$

where SS ($\overline{\mathrm{SS}}$) indicates that the system is (is not) using the pioneer beacon setup and the descriptions of the σ^2's are as follows:

- σ_{band}^2: bandwidth limitation induced wavefront variance;
- σ_{path}^2: temporal and spatial anisoplanatism induced wavefront variance;
- σ_{d}^2: chromatic effect on the diffraction pattern induced wavefront variance;
- σ_{ch}^2: chromatic path length error induced wavefront variance; and
- σ_{ϕ}^2: chromatic anisoplanatism induced wavefront.

Details of the calculations and expressions of these σ^2's can be found in the Appendix from Eq. (A1) to Eq. (A11). Note that $v_{\mathrm{app}}(h)$ cannot be reduced by using the pioneer beacon setup. The AO system still "sees" a fast-changing beacon. This is reflected in the wavefront variance due to bandwidth σ_{band}^2. The significance of our design is the improvement on σ_{path}^2. As the aim of this subsection is to compare different multiplexing methods, we ignore system degradation due to factors that are not related to temporal, chromatic, or anisoplanatic effects in our calculation. Furthermore, for simplicity, we do not take interlacing into account for all TDM calculations in this paper.

Figure 5 shows the results of the calculation. For both $h_{\mathrm{alt}} = 400$ and 800 km, the Strehl ratio of the TDM system is higher than that of the WDM system, which, in turn, is much higher than when AO is turned off for all zenith angles ζ. More importantly, for $h_{\mathrm{alt}} = 400$ km, separating the beacon and the signal beams up to $L = 5$ m gives higher S than the TDM system when $\zeta \lesssim 60°$. For $h_{\mathrm{alt}} = 800$ km, separating the two beams up to $L = 5$ m always gives a higher S than the TDM system when $\zeta \lesssim 55°$. This means that anisoplanatism is the dominant factor when calculating the Strehl ratio.

B. Channel efficiency

The total efficiency η of the satellite-to-ground channel, which depends on the atmospheric condition, can be expressed as[21,26]

$$\eta = \eta_{\mathrm{trans}}(\zeta)\eta_{\mathrm{rec}}\eta_{\mathrm{spec}}\eta_{\mathrm{det}}\eta_{\mathrm{geo}}(\zeta)\eta_{\mathrm{FS}}(\zeta). \tag{24}$$

Here, factors that implicit or explicit depend on the zenith angle ζ are emphasized by explicitly showing this dependence. In Eq. (24), $\eta_{\mathrm{trans}}(\zeta)$ is the free-space transmission efficiency. It depends on the zenith angle ζ although the dependence is rather weak. To simplify matter, we assume that η_{trans} is a linear function of ζ with $\eta_{\mathrm{trans}} = 0.92$ at $\zeta = 0°$ and $\eta_{\mathrm{trans}} = 0.74$ at $\zeta = 75°$. These two values are the results obtained by Gruneisen *et al.* in their the MODTRAN simulation for clear sky conditions.[26] Actually, we have tried a few

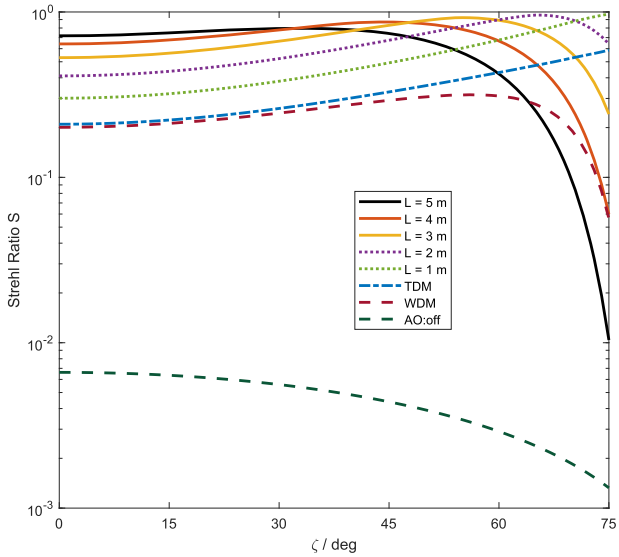

(a) $h_{\text{alt}} = 400$ km

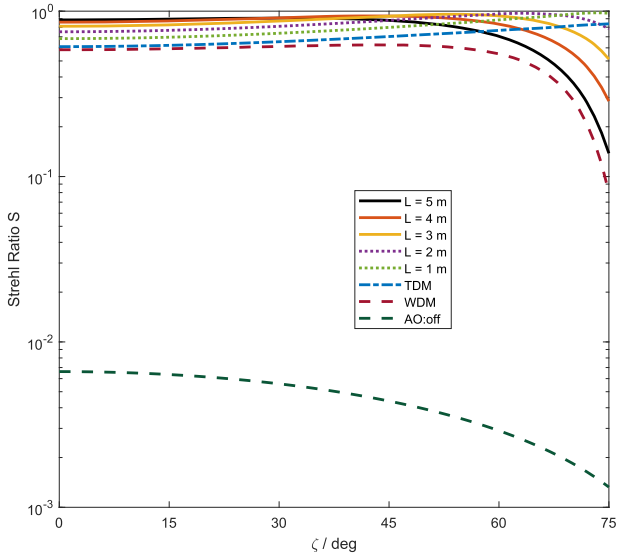

(b) $h_{\text{alt}} = 800$ km

FIG. 5. Strehl ratio S of different system configurations as a function of zenith angle ζ. The black solid, red solid, yellow solid, purple dotted, and green dotted curves are computed with $D = 1.03$ m and spatial separation L being 5, 4, 3, 2, and 1 m, respectively. The blue dashed-dotted and brown dashed curves are for pure TDM and WDM methods, respectively. The dark green dashed curve is for turning off AO.

variations on η_{trans} and found that it does not change our results in any significant way. As for the other factors in Eq. (24), we follow Lanning *et al.*[21] by picking the efficiency of the receiver $\eta_{\text{rec}} = 0.5$, the efficiency of the spectral filter $\eta_{\text{spec}} = 0.9$, and the detector efficiency $\eta_{\text{det}} = 0.8$. In addition, the aperture-to-aperture coupling efficiency $\eta_{\text{geo}}(\zeta)$ is given by Eq. (10), and the efficiency of the FS is given by[21]

$$\eta_{\text{FS}}(\zeta) = 0.84S. \tag{25}$$

Note that η_{FS} implicitly depends on the zenith angle ζ through the Strehl ratio S.

We find from Fig. 6 that the total transmission efficiency η always decreases as the zenith angle ζ increases. This is what we expect. Note further that η_{FS} is the only factor that is related to the distortion loss in this framework. From Eq. (25), a higher Strehl ratio S implies a higher η. Thus, Fig. 6 shows that the aperture coupling efficiency plays a significant role as the altitude increases. Higher altitude can decrease the anisoplanatism, but the total channel transmission efficiency η decreases due to larger the beam size spread. Figure 6 also depicts that for $L \leq 5$ m, η increases with L when the zenith angle $\zeta \lesssim 30°$.

VI. APPLICATION IN QUANTUM KEY DISTRIBUTION

We now consider the effect of crosstalk between the beacon and signal beams. To analyze the effectiveness of our protocol, we choose the most extreme setting that the signal beam is a weak coherent photon source used in decoy state BB84 QKD using three photon intensities,[27–29] namely, the vacuum source and two phase randomized Poissonian distributed sources with intensities μ and ν. In this setting, crosstalk noise could affect the system seriously by increasing the quantum bit error rate (QBER) and, hence, lowering the secret key rate. In this regard, if our protocol works better than existing satellite-to-ground QKD setups, then it should also work in practically all realistic satellite-to-ground communication, both classical and quantum.

Recall that the background detection probability can be written as

$$Y_0 = (N_b + N_{\text{cross}})\eta_{\text{spec}}\eta_{\text{rec}}\eta_{\text{det}} + 4f_{\text{dark}}\Delta t, \tag{26}$$

where N_b, N_{cross}, f_{dark}, and Δt are the sky photon noise, crosstalk noise due to the beacon, the dark count rate of the detectors, and the detection time window, respectively. Moreover, N_b is calculated using Eq. (18) with the parameters stated in Table I. As a conservative estimate, we assume that N_{cross} is 100 times of the scattering noise calculated in Sec. IV C when spatial multiplexing is used. Furthermore, for WDM and TDM systems, we take the liberty to set $N_{\text{cross}} = 0$. The rest of the calculations are well known and can be found in the work of Ma *et al.*[29] We include them here for readers' convenience. The QBER can be expressed as

$$E_\mu = \frac{e_0 Y_0 + e_d(1 - e^{-\eta\mu})}{Y_0 + 1 - e^{-\eta\mu}}, \tag{27}$$

where e_0 and e_d are the system noise error rate and polarization crosstalk. The value of the parameters are based on those used by Lanning *et al.*[21] and are presented in Table I. These parameters are optimized to give the highest possible secret key rate for free-space photon transmission in the so-called asymptotic limit, namely, for the case of an arbitrarily large number of photon transfer. The secret key rate (more accurately, a provably secure lower

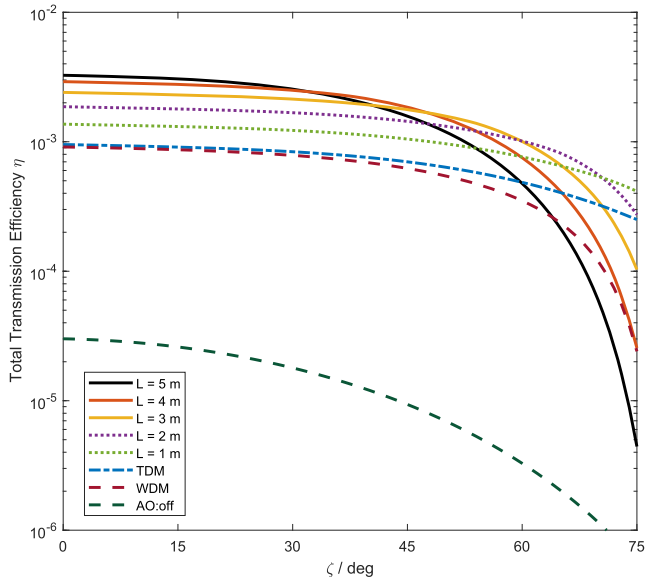

(a) $h_{\text{alt}} = 400$ km

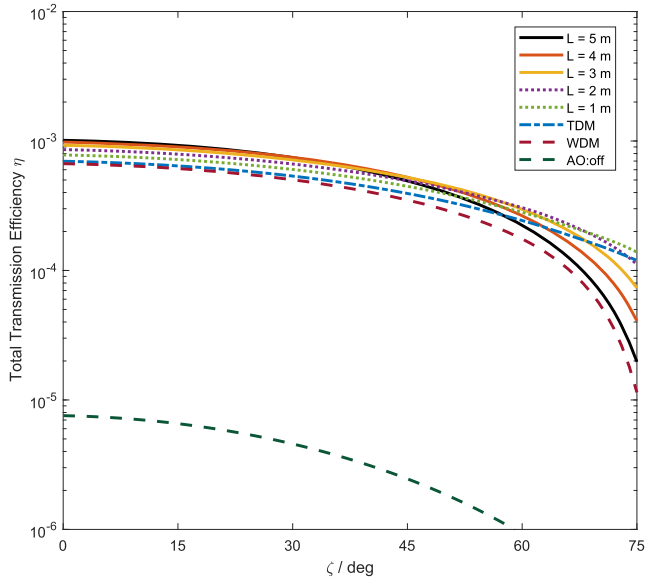

(b) $h_{\text{alt}} = 800$ km

FIG. 6. Total transmission efficiency η of different system configurations as a function of zenith angle ζ. The curves are labeled in the same way as in Fig. 5.

bound of the number of secret key obtained at the end divided by the number of signal photon pulses emitted by the satellite) can be written as

$$R \geq q\{e^{-\mu}\mu Y_1[1 - h_2(e_1)] - f_e Q_\mu h_2(E_\mu)\}, \tag{28}$$

TABLE I. Parameters used for calculating the secret key rate of the decoy state BB84 protocol used by Lanning *et al.*[21]

QKD parameters		
Quantity	Symbol	Value
Signal-state mean photon numbers	μ	0.7
Decoy-state mean photon numbers	ν	0.1
Repetition rate	f_{source}	10 MHz
Sky radiance	H_b	25 W m^{-2} sr μm
Dark count rate	f_{dark}	10 Hz
Polarization crosstalk	e_d	0.01
System noise error	e_0	0.5
Spectral filter bandpass	$\Delta\lambda$	0.2 nm
Detection time	Δt	1 ns
Error-correction efficiency	f_e	1.22

where $h_2(x)$ is the binary entropy function, Y_1 is the single photon state yield,

$$Y_1 = \frac{\mu}{\mu\nu - \nu^2}\left(Q_\nu e^\nu - Q_\mu e^\mu \frac{\nu^2}{\mu^2} - \frac{\mu^2 - \nu^2}{\mu^2} Y_0\right), \tag{29}$$

e_1 is the single photon state error rate,

$$e_1 = \frac{Q_\nu E_\nu e^\nu - e_0 Y_0}{Y_1 \nu}, \tag{30}$$

and Q_μ is the gain at intensity μ,

$$Q_\mu = Y_0 + 1 - e^{-\eta\mu}. \tag{31}$$

Finally, q is the probability that the trusted agents on the satellite and on the ground use the same basis for preparing and measuring their signal photons in their QKD experiment. In the work of Lanning *et al.*,[21] q is chosen to be 1/2. However, in the asymptotic limit, the optimized key rate can be computed by taking the limit of $q \to 1$ using biased bases selection.[30] Note, however, that as q is a parameter independent of the channel and the AO setup used. It only appears as a multiplication factor in the RHS of Eq. (28) as far as the key rate is concerned. Consequently, if the key rate of a certain method is higher than that of another method for a fixed $q > 0$, then the key rate of the former method is always higher than the later for all $q \in (0, 1]$. Therefore, we only need to compare the provably secure key rates of different methods by fixing, say, $q = 1/2$.

While theorists use a dimensionless key rate, such as the one in Eq. (28), as one of the effectiveness metric to study QKD protocols, from a practical point of view, here we use the "experimentalist" version of the key rate, namely, $f_{\text{source}}R$ in this study. It tells us the lower bound of the number of provably secure secret key bits generated per unit time. Figures 7 and 8 show the final results of the QBER and the "experimentalist" version of the key rate. By comparing Fig. 5 with Fig. 7, we find that QBER is anti-correlated with S. This is not surprising as high aberration is likely to cause higher detection error. In fact, our result suggests that aberration is the main source of quantum bit error in our system. In other words, the high QBER is caused by low signal to noise ratio as more and

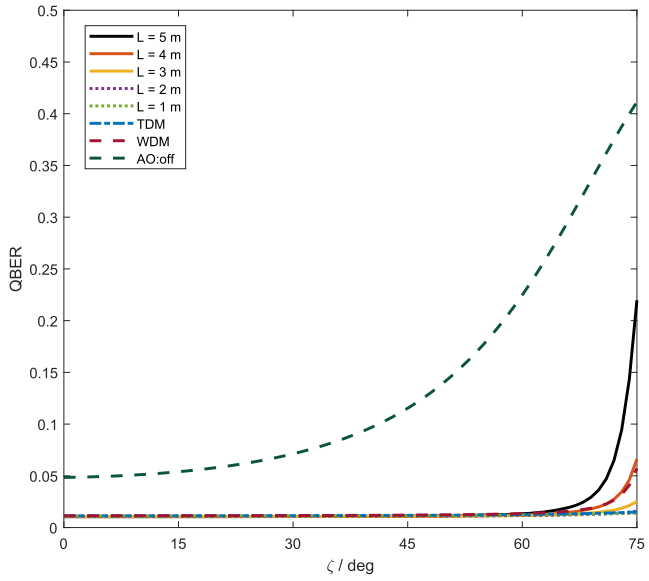

(a) $h_{\text{alt}} = 400$ km

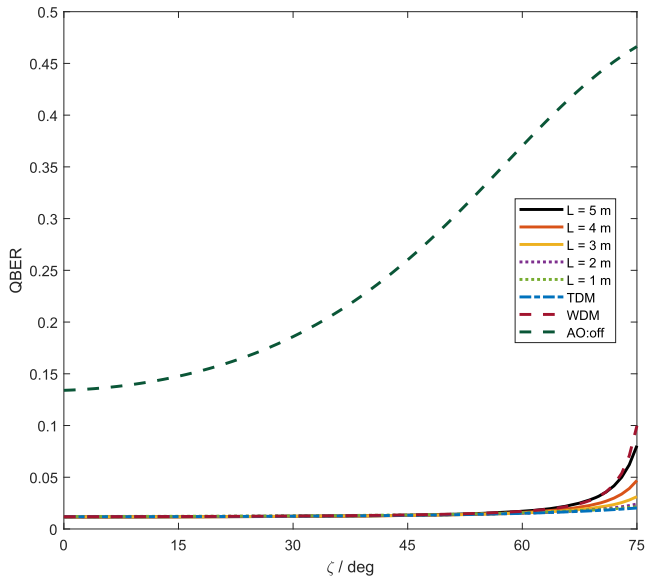

(b) $h_{\text{alt}} = 800$ km

FIG. 7. QBERs of different system configurations. The curves are labeled in the same way as in Fig. 5.

more signal detected is from noise. For the key rate, Fig. 8 depicts that the curves of the AO systems have the same pattern as the total channel efficiency for $\zeta \lesssim 65°$. This is because the QBER is more or less a constant for a given L. Furthermore, Fig. 8 shows that QKD is not possible by turning off AO. More importantly, for $\zeta \lesssim 55°$, the key rate of using pioneer beacon beam plus AO is higher than that of the TDM system, which, in turn, is higher than that of the WDM system. Comparing to the TDM system, at altitude $h_{\text{alt}} = 400$ km and zenith angle $\zeta \leq 30°$, the improvements are at

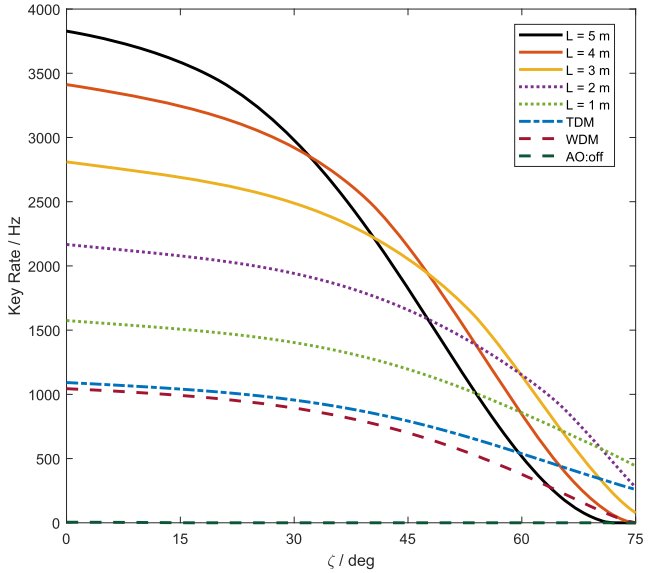

(a) $h_{\text{alt}} = 400$ km

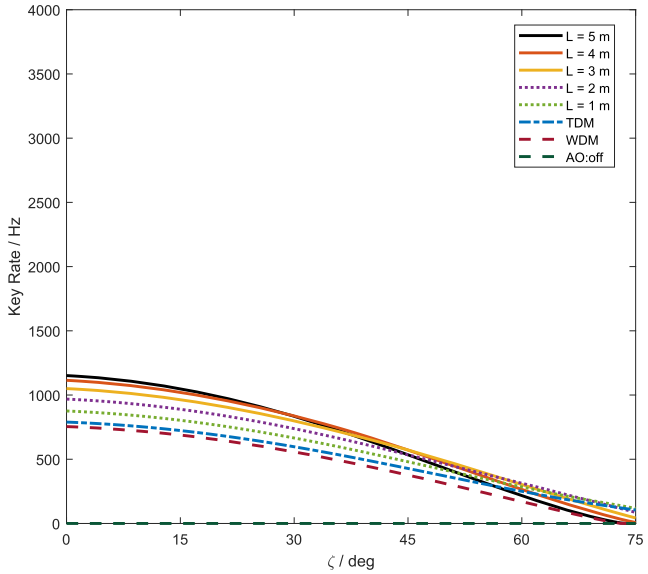

(b) $h_{\text{alt}} = 800$ km

FIG. 8. Provably secure key rates of different system configurations. The curves are labeled in the same way as in Fig. 5. Note that the key rate of pure WDM and pure TDM systems is 0 Hz when $h_{\text{alt}} = 400$ km, while the key rate is close to 0 Hz when AO is not used and ζ is small.

least 215% and 47% for $L = 5$ and 1 m, respectively. Whereas for $h_{\text{alt}} = 800$ km, the corresponding improvements are 40% and 11%, respectively. These improvement figures are computed by setting the response time T_r, which is inversely proportional to the bandwidth of the system. For systems with lower bandwidth, there are more rooms for improvement as the temporal angle is larger. We can further increase L to obtain a more significant key rate improvement.

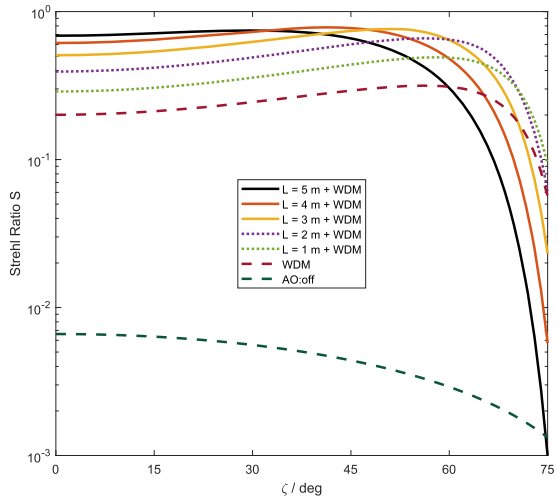

(a) $h_{\text{alt}} = 400$ km

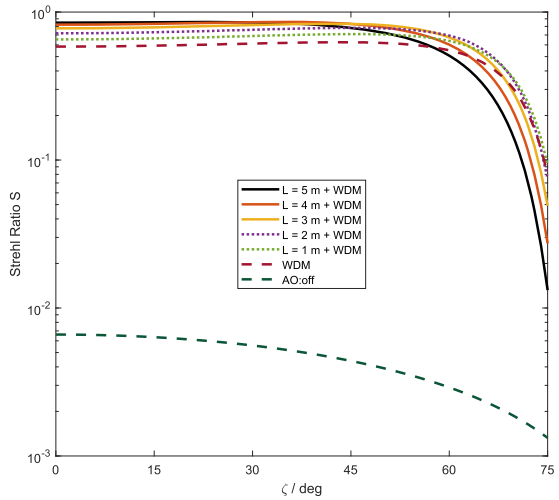

(b) $h_{\text{alt}} = 800$ km

FIG. 9. Strehl ratio of WDM systems. Similar to the labeling scheme in Fig. 5, the black solid, red solid, yellow solid, purple dotted, and green dotted curves are computed using $D = 1.03$ m and WDM with spatial separation L being 5, 4, 3, 2, and 1 m, respectively. The brown dashed curve is for the pure WDM method. Finally, the dark green dashed curve is for turning off AO.

VII. IMPROVING WDM SYSTEMS USING A PIONEER BEACON

As WDM is a popular method to combine the beacon and signal beams, it is easier to upgrade the system with a pioneer beacon than building a spatial multiplexing system. Here, we present the

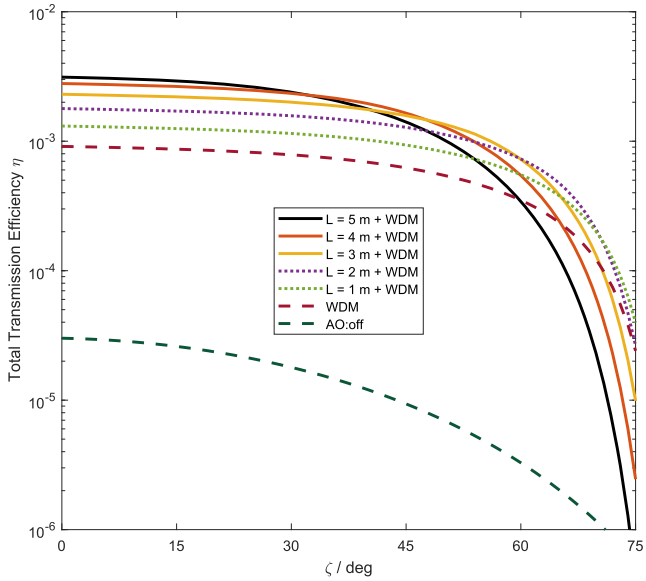

(a) $h_{\text{alt}} = 400$ km

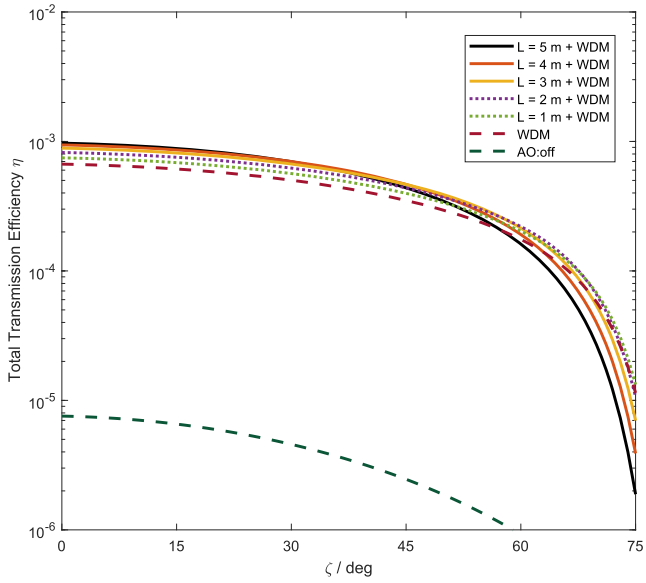

(b) $h_{\text{alt}} = 800$ km

FIG. 10. Total transmission efficiency η of WDM systems. The curves are labeled in the same way as in Fig. 9.

improvement to WDM systems with our idea. To study that, we modify Eq. (23) to[3]

$$\sigma^2_{\mathrm{WDM}} = \sigma^2_{\mathrm{band}} + \sigma^2_{\mathrm{path,SS}} + \sigma^2_{\mathrm{d}} + \sigma^2_{\mathrm{ch}} + \sigma^2_{\phi}. \tag{32}$$

Using the same set of parameters and following the same analysis in Secs. V and VI, the Strehl ratio, QBER, and key rate are shown in Figs. 9–12, respectively. We remark that the curves, including their shapes and trends, in these figures are very similar to those in Figs. 5–8. In other words, the performance of our improvement to the WDM system is similar to that of the spatial multiplexing one.

In summary, upgrading a pure WDM system with a pioneer beacon beam can significantly increase the secret key rate in decoy

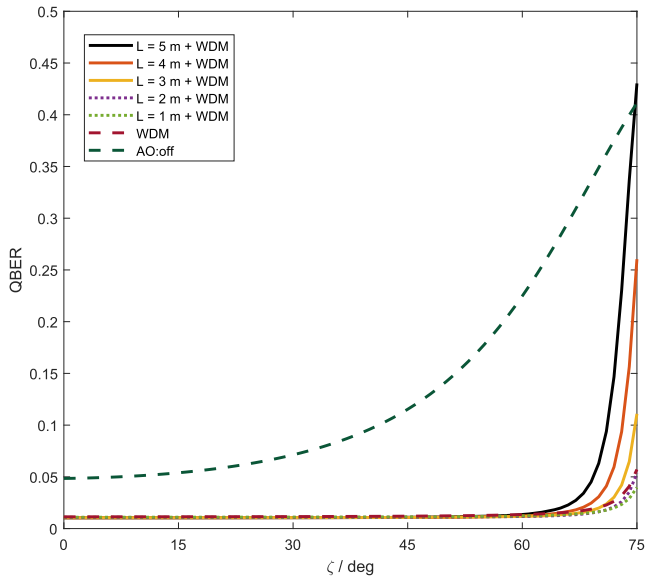

(a) $h_{\mathrm{alt}} = 400$ km

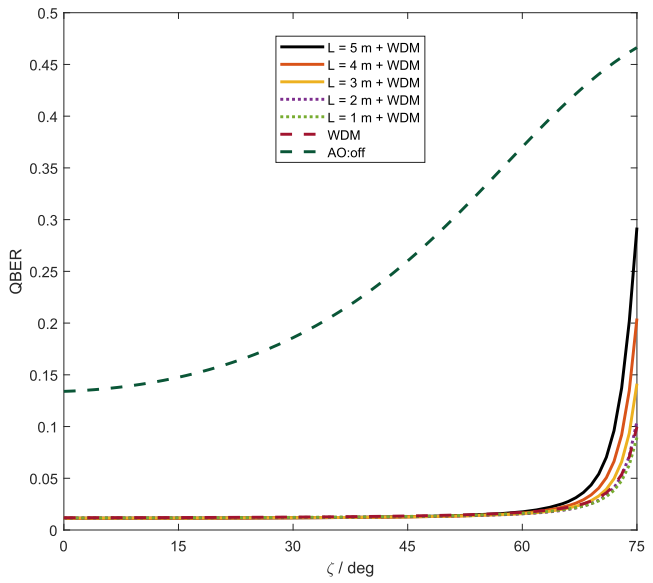

(b) $h_{\mathrm{alt}} = 800$ km

FIG. 11. QBER of WDM systems. The curves are labeled in the same way as in Fig. 9.

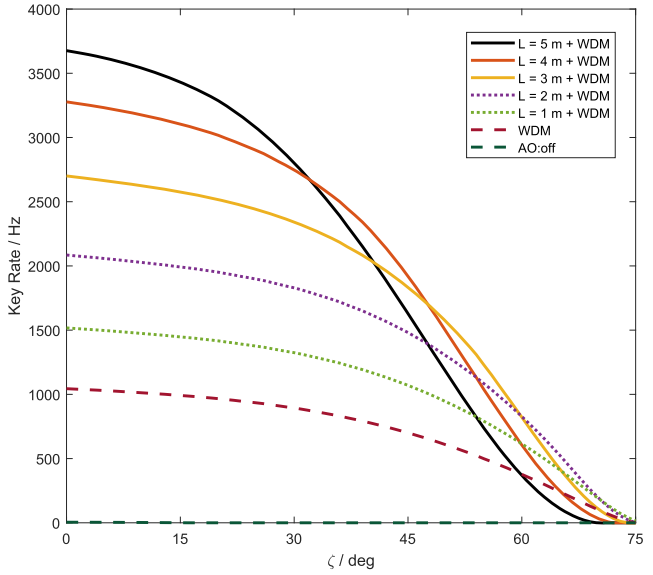

(a) $h_{\mathrm{alt}} = 400$ km

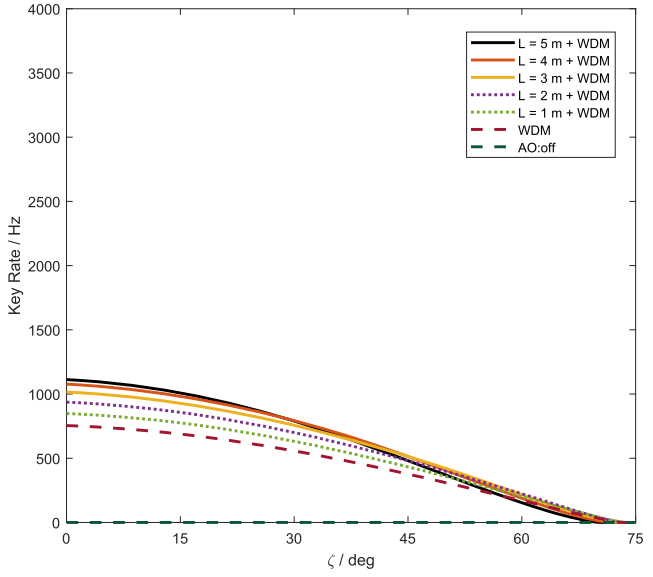

(b) $h_{\mathrm{alt}} = 800$ km

FIG. 12. Key rate of WDM systems. The curves are labeled in the same way as in Fig. 9. Note that when AO is off, the key rate is 0 Hz except when $h_{\mathrm{alt}} = 400$ km and ζ is low.

state QKD using the phase-randomized Poissonian source. Furthermore, by comparing Fig. 8 with Fig. 12, for the same value of L, the two systems have comparable key rates for $\zeta < 45^\circ$—the latter is at least 90% of the former. Again, these improvement figures are computed by setting the response time T_r, which is inversely proportional to the bandwidth of the system. For systems with lower bandwidth, there are more rooms for improvement as the temporal angle is larger. We can further increase L to obtain a more significant key rate improvement. In summary, our results imply that upgrading existing WDM systems is a very attractive alternative to building entirely new spatial multiplexing ones.

VIII. CONCLUSIONS

In this paper, we report a method to apply AO technologies to optical communication systems. The main ideas are the spatial separation of the beacon and the signal beam. For fast-moving sources, our design, which in essence performs time-based AO precompensation, can reduce the angle between the optical paths of the beacon and the corresponding signal. Thus, it can reduce the anisoplanatism of the AO correction. We estimate the crosstalk caused by the diffraction and the scattering of the beacon. As there is a field stop in the beacon receiving module and the power of the beacon is not high, the crosstalk by the beacon can be neglected. By the semi-empirical study, we show that the key rate of our scheme in LEO satellite-to-ground QKD is better than the pure TDM and WDM methods. For zenith angle $\zeta \le 30^\circ$, the improvement is up at least 215% for beam separation $L = 5$ m on a 400 km altitude satellite using a response time T_r of 3 dB of the whole system response bandwidth. We also find that the lower the bandwidth, the higher the key rate improvement. We also consider an alternative system that adds a pioneer beacon beam to existing pure WDM systems. We find that for the zenith angle less than about 45°, this alternative setup performs QKD at a rate of at least 90% of our original proposal, making it an attractive engineering option, in practice. Further analysis of the system performance can be found in the Master thesis of one of the authors.[16] We are going to report the effects of fine tuning the delay time T_r and beam separation L in our follow up work. Finally, we stress that our method is also applicable to classical optical free-space communication as we do not any quantum property of the signal source.

ACKNOWLEDGMENTS

We would like to thank Hoi-Kwong Lo, Alan Pak Tao Lau, Chengqiu Hu, Wenyuan Wang, and Gai Zhou for the discussion in optics. This work was supported by RGC Grant No. 17302019 of the Hong Kong SAR Government.

AUTHOR DECLARATIONS

Conflict of Interest

This paper is related to a patent application submitted by the authors.

Author Contributions

Kai Sum Chan: Conceptualization (supporting); Formal analysis (lead); Investigation (equal); Methodology (lead); Software (lead); Visualization (lead); Writing – original draft (lead); Writing – review & editing (supporting). **H. F. Chau**: Conceptualization (lead); Formal analysis (supporting); Funding acquisition (lead); Investigation (equal); Methodology (supporting); Project administration (lead); Supervision (lead); Validation (lead); Writing – original draft (supporting); Writing – review & editing (lead).

DATA AVAILABILITY

The data that support the findings of this study are available from the corresponding author upon reasonable request.

APPENDIX: WAVEFRONT VARIANCE CALCULATION

The calculation here is based on Tyson and Frazier's book[3] and the paper by Devaney *et al.*[25] First, we consider the variance caused by the limitation of the bandwidth of the AO system. It can be written as[3]

$$\sigma^2_{\text{band}} = \int_0^\infty |1 - H(f, f_c)|^2 F(f)\, df, \tag{A1}$$

where $f_c = 500$ Hz is the bandwidth of the AO system, f is a frequency variable,

$$H(f, f_c) = \left(1 + \frac{if}{f_c}\right)^{-1} \tag{A2}$$

is the RC filter that used to model the system, and

$$F(f) = 0.0326k^2 f^{-8/3} \int_0^{z(\zeta)} v^{5/3}(z) C_n^2(z)\, dz \tag{A3}$$

is the power spectrum of the turbulence frequency. Here, $v(z)$ is the wind speed calculated using Eq. (3). Note that the bandwidth-limited wavefront variance is the same for all AO systems studied in this paper.

Next, we discuss the chromatic effects that appears in WDM systems. The first contribution of chromatic aberration is due to diffraction. The diffraction pattern of the beams at the receiving end depends on the wavelength.[25] When the beacon wavelength is λ_b, the variance on measuring the signal beam with wavelength λ is[25]

$$\sigma_{\text{d}}^2 = \frac{4.08}{\pi} k^2 \int_0^L \int_0^\infty K^{-8/3} \left\{1 - \left(\frac{4}{KD}\right)^2 \left[J_1\left(\frac{KD}{2}\right)\right]^2\right\} \times \left[\cos\left(\frac{zK^2}{2k_b}\right) - \cos\left(\frac{zK^2}{2k}\right)\right]^2 C_n^2(z)\, dz\, dK, \tag{A4}$$

where K is the spatial frequency and $k_b = 2\pi/\lambda_b$ is the wavenumber of the beacon. The second chromatic contribution comes from path length error between the beams. A DM is only able to compensate error perfectly at a single wavelength. This is because there is a path length difference between light beams with different wavelengths. The corresponding wavefront variance is[25]

$$\sigma^2_{\text{ch}} = 1.03 \left(\frac{D}{r_0}\right)^{5/3} \epsilon^2(\lambda, \lambda_b), \tag{A5}$$

where

$$\epsilon(\lambda, \lambda_b) = \frac{\lambda_b}{\lambda} \frac{n_s(\lambda) - n_s(\lambda_b)}{n_s(\lambda_b) - 1}. \tag{A6}$$

In the above equation, n_s is the refractive index, which is calculated at standard pressure and temperature base on Ciddor's model.[31]

Finally, we calculate the wavefront variance caused by chromatic anisoplanatism. Light waves with different wavelength travel different paths because of dispersion. The isoplanatic error induced by this can be written as[25]

$$\sigma_\phi^2 = \left[\frac{\sin(\zeta)\Delta n}{\cos^2(\zeta)}\right]^{5/3} T_{5/3}, \tag{A7}$$

where

$$\Delta n = |n_s(\lambda) - n_s(\lambda_b)| \tag{A8}$$

is the difference in refractive index and

$$T_{5/3} = 2.91 k_b^2 \sec(\zeta) \int_0^{h_{\text{alt}}} I^{5/3}(h) C_n^2(h)\, dh, \tag{A9}$$

with $I(h)$ being equal to the integral of the air density normalized to the value at sea level,

$$I(h) = \int_0^h \alpha(z)\, dz. \tag{A10}$$

For simplicity, we only take integral of the troposphere in this paper as this layer contributes most to $I(h)$. Specifically, we follow the website of Shelquist[32] by using the air density model,

$$h(\rho) = 44\,330.8 - 42\,266.5\rho^{0.234\,969} \tag{A11}$$

for $h \le 1.1 \times 10^4$ m^2, where ρ is measured in unit of kg/m^3. Clearly, $h(\rho)$ is an invertible function. By denoting its inverse function by $\rho(h)$, then $\alpha(h)$ is simply $\rho(h)/\rho(0)$.

REFERENCES

[1] *Principles of Adaptive Optics*, edited by F. Roddier (CUP, Cambridge, 2009).
[2] O. Guyon, Annu. Rev. Astron. Astrophys. **56**, 315 (2018).
[3] R. K. Tyson and B. W. Frazier, *Principles of Adaptive Optics*, 5th ed. (CRC Press, New York, 2022).
[4] Y. Wang, H. Xu, D. Li, R. Wang, C. Jin, X. Yin, S. Gao, Q. Mu, L. Xuan, and Z. Cao, Sci. Rep. **8**, 1124 (2018).
[5] Y. Cao, Y.-H. Li, K.-X. Yang, Y.-F. Jiang, S.-L. Li, X.-L. Hu, M. Abulizi, C.-L. Li, W. Zhang, Q.-C. Sun, W.-Y. Liu, X. Jiang, S.-K. Liao, J.-G. Ren, H. Li, L. You, Z. Wang, J. Yin, C.-Y. Lu, X.-B. Wang, Q. Zhang, C.-Z. Peng, and J.-W. Pan, Phys. Rev. Lett. **125**, 260503 (2020).
[6] M. T. Gruneisen, M. L. Eickhoff, S. C. Newey, K. E. Stoltenberg, J. F. Morris, M. Bareian, M. A. Harris, D. W. Oesch, M. D. Oliker, M. B. Flanagan, B. T. Kay, J. D. Schiller, and R. N. Lanning, Phys. Rev. Appl. **16**, 014067 (2021).
[7] P. L. Wizinowich, D. Le Mignant, A. H. Bouchez, R. D. Campbell, J. C. Y. Chin, A. R. Contos, M. A. van Dam, S. K. Hartman, E. M. Johansson, R. E. Lafon, H. Lewis, P. J. Stomski, D. M. Summers, C. G. Brown, P. M. Danforth, C. E. Max, and D. M. Pennington, Publ. Astron. Soc. Pac. **118**, 297 (2006).
[8] J. Osborn, M. J. Townson, O. J. D. Farley, A. Reeves, and R. M. Calvo, Opt. Express **29**, 6113 (2021).
[9] S. Walsh and S. Schediwy, Opt. Lett. **48**, 880 (2023).
[10] F. Bennet, I. Price, F. Rigaut, and M. Copeland, in Advanced Maui Optical and Space Surveillance Technologies Conference, 2016, poster presentation, source available in https://www.semanticscholar.org/paper/Satellite-Imaging-with-Adaptive-Optics-on-a-1-M-Bennet-Price/21541a3038bec1a04e668afd29135282053e263e.
[11] S. Pirandola, U. L. Andersen, L. Banchi, M. Berta, D. Bunandar, R. Colbeck, D. Englund, T. Gehring, C. Lupo, C. Ottaviani, J. L. Pereira, M. Razavi, J. Shamsul Shaari, M. Tomamichel, V. C. Usenko, G. Vallone, P. Villoresi, and P. Wallden, Adv. Opt. Photonics **12**, 1012 (2020).
[12] S.-K. Liao, W.-Q. Cai, W.-Y. Liu, L. Zhang, Y. Li, J.-G. Ren, J. Yin, Q. Shen, Y. Cao, Z.-P. Li, F.-Z. Li, X.-W. Chen, L.-H. Sun, J.-J. Jia, J.-C. Wu, X.-J. Jiang, J.-F. Wang, Y.-M. Huang, Q. Wang, Y.-L. Zhou, L. Deng, T. Xi, L. Ma, T. Hu, Q. Zhang, Y.-A. Chen, N.-L. Liu, X.-B. Wang, Z.-C. Zhu, C.-Y. Lu, R. Shu, C.-Z. Peng, J.-Y. Wang, and J.-W. Pan, Nature **549**, 43 (2017).
[13] F. Xu, X. Ma, Q. Zhang, H.-K. Lo, and J.-W. Pan, Rev. Mod. Phys. **92**, 025002 (2020).
[14] M. T. Gruneisen, B. A. Sickmiller, M. B. Flanagan, J. P. Black, K. E. Stoltenberg, and A. W. Duchane, Proc. SPIE **9254**, 925404 (2014).
[15] K. S. Chan and H. F. Chau, "Improving classical and quantum free-space communication by adaptive optics and by separating the reference and signal beams with time delay for source(s) moving relative to the detector(s)," patent application PCT/CN2021/096100 and PCT/CN2022/094917 (25 May 2022).
[16] K. S. Chan, "Improving quantum key distribution by adaptive optics," M.S. thesis, University of Hong Kong, 2022.
[17] D. L. Fried, J. Opt. Soc. Am. **55**, 1427 (1965).
[18] R. E. Hufnagel and N. R. Stanley, J. Opt. Soc. Am. **54**, 52 (1964).
[19] D. P. Greenwood, J. Opt. Soc. Am. **67**, 390 (1977).
[20] R. J. Sasiela, *Electromagnetic Wave Propagation in Turbulence: Evaluation and Application of Mellin Transforms, 2nd ed.* (SPIE Publications, 2007).
[21] R. N. Lanning, M. A. Harris, D. W. Oesch, M. D. Oliker, and M. T. Gruneisen, Phys. Rev. Appl. **16**, 044027 (2021).
[22] See http://www.lulin.ncu.edu.tw/instrument/LOT/ for Lulin Observatory website; acccessed 28 April 2022.
[23] *The WSPC Handbook of Astronomical Instrumentation*, edited by D. N. Burrows (World Scientific, Singapore, 2020), Vols. 2 and 3.
[24] E.-L. Miao, Z.-F. Han, S.-S. Gong, T. Zhang, D.-S. Diao, and G.-C. Guo, New J. Phys. **7**, 215 (2005).
[25] N. Devaney, A. V. Goncharov, and J. C. Dainty, Appl. Opt. **47**, 1072 (2008).
[26] M. T. Gruneisen, M. B. Flanagan, and B. A. Sickmiller, Opt. Eng. **56**, 126111 (2017).
[27] X.-B. Wang, Phys. Rev. Lett. **94**, 230503 (2005).
[28] H.-K. Lo, X. Ma, and K. Chen, Phys. Rev. Lett. **94**, 230504 (2005).
[29] X. Ma, B. Qi, Y. Zhao, and H.-K. Lo, Phys. Rev. A **72**, 012326 (2005).
[30] H.-K. Lo, H. F. Chau, and M. Ardehali, J. Cryptology **18**, 133 (2005).
[31] P. E. Ciddor, Appl. Opt. **35**, 1566 (1996).
[32] R. Shelquist, "An introduction to air density and density altitude calculations," https://wahiduddin.net/calc/density_altitude.htm; acccessed 1 October 2022 (2019).